Journal of Magnetism and Magnetic Materials 451 (2018) 443–449

Contents lists available at ScienceDirect

Journal of Magnetism and Magnetic Materials

journal homepage: www.elsevier.com/locate/jmmm

Research articles

Spin-wave dynamics and exchange interactions in multiferroic $NdFe_3(BO_3)_4$ explored by inelastic neutron scattering

I.V. Golosovsky [a,*], A.K. Ovsyanikov [a,b], D.N. Aristov [a], P.G. Matveeva [a], A.A. Mukhin [c], M. Boehm [d], L.-P. Regnault [e], L.N. Bezmaternykh [f]

[a] National Research Center "Kurchatov Institute", B.P. Konstantinov Petersburg Nuclear Physics Institute, 188300 Gatchina, Russia
[b] Peter the Great St. Petersburg Polytechnic University, 195251 St. Petersburg, Russia
[c] Prokhorov General Physics Institute, RAS, 119991 Moscow, Russia
[d] Institut Laue Langevin, 71 avenue des Martyrs, 38042 Grenoble, France
[e] SPSMS, UMR-E CEA/UJF-Grenoble 1, INAC, 38054 Grenoble, France
[f] Kirensky Institute of Physics, Siberian Division of RAS, 660036 Krasnoyarsk, Russia

ARTICLE INFO

Article history:
Received 25 April 2017
Received in revised form 15 October 2017
Accepted 18 October 2017
Available online 19 October 2017

Keywords:
Inelastic neutron diffraction
Magnons
Exchange interactions

ABSTRACT

Magnetic excitations and exchange interactions in multiferroic $NdFe_3(BO_3)_4$ were studied by inelastic neutron scattering in the phase with commensurate antiferromagnetic structure. The observed spectra were analyzed in the frame of the linear spin-wave theory. It was shown that only the model, which includes the exchange interactions within eight coordination spheres, describes satisfactorily all observed dispersion curves. The calculation showed that the spin-wave dynamics is governed by the strongest antiferromagnetic intra-chain interaction and three almost the same inter-chain interactions. Other interactions, including ferromagnetic exchange, appeared to be insignificant. The overall energy balance of the antiferromagnetic inter-chain exchange interactions, which couple the moments from the adjacent ferromagnetic layers as well as within a layer, stabilizes ferromagnetic arrangement in the latter. It demonstrates that the pathway geometry plays a crucial role in forming of the magnetic structure.

1. Introduction

The discovery of the multiferroics, which possess magnetic order and electric polarization order, refers to the 60-s of the last century. However, the magnetoelectric coupling in these compounds turned out to be relatively weak [1]. It took decades until the discovery in 2003 of the rare earth manganite $RMnO_3$ [2], with strong coupling between electric and magnetic subsystems, introduced the concept of spin-driven ferroelectricity and brought about the revival of the research activity in the multiferroics.

Competition of exchange interactions, which leads to incommensurate magnetic structure and induces electric polarization is a characteristic of these compounds [3,4]. Similar magnetoelectric phenomena were found soon in other compounds with incommensurate magnetic order: manganites RMn_2O_5 [5,6], vanadates $Ni_3V_2O_8$ [7], tungstate $MnWO_4$ [8] and others. Extensive efforts were made to create films of multiferroics, which are very promising for applications [9].

Relatively recently a new family of the rare-earth multiferroics, known as ferroborates $RFe_3(BO_3)_4$ and alumoborates $RAl_3(BO_3)_4$ attracted significant attention due to their very strong magnetoelectric effect [10–14]. In contrast to the manganites, these compounds have non-centrosymmetric crystal structure (space group R32 or $P3_121$), so the electric polarization is not related to incommensurate magnetic order, but is induced by the collinear magnetic ordering in the sublattice of iron or by an external magnetic field. In ferroborates, where a strong Fe-Fe interaction determines the Néel temperature (30–40 K), R-Fe exchange and anisotropy of the rare-earth subsystem plays an important role. Rare earth ions provide the main contribution to the magnetoelectric properties as evidenced by the strong dependence of the electric polarization on the type of rare earth ion [15].

The magnetic order and its impact on the electric order are determined by the exchange interaction and the magnetic anisotropy. Therefore, the knowledge of magnetic Hamiltonian parameters is crucial for examining the mechanisms behind the multiferroic properties. These parameters could be acquired from the spin-wave spectrum.

* Corresponding author.
E-mail address: golosovsky_iv@pnpi.nrcki.ru (I.V. Golosovsky).

https://doi.org/10.1016/j.jmmm.2017.10.065
0304-8853/

The spectrum of magnetic excitations is important for the understanding of the coupled excitations, responsible for the coupling of magnetic and electric subsystems, known as electromagnons [16]. Electromagnons can be interpreted as electrically active spin waves, which give a resonant contribution to the dielectric permittivity due to the strong spin-lattice interaction. Recently, it was found that the low-frequency AFMR mode in $Sm_{1-x}La_xFe_3(BO_3)_4$, which corresponds to an in-plane spin wave, represents an electromagnon [17–19].

There are few experimental works on magnons in multiferroics. It should be noted the work on classical multiferroic $BiFeO_3$ [20], where the spin-wave spectra were measured in the whole Brillouin zone. As for other compounds, there are several publications on inelastic neutron scattering. In the first papers on tungstates $MnWO_4$ [21,22], based on the model, which includes the Heisenberg isotropic exchange and uniaxial anisotropy, analytical expressions for the dispersion relations in spin-wave approximation were acquired. It should be noted a number of works on multiferroics $RMnO_3$ [22–24]. One should mark the work of D. Senff et. al. [25], in which, using inelastic neutron scattering, the spin excitations in $TbMnO_3$ and the relation of some spin modes with the electromagnons were established.

Concerning ferroborates, only recently, the dispersion of the magnons throughout the Brillouin zone was published [26]. Before, the only information about the magnetic excitations in these compounds was obtained by Terahertz, Raman, AFMR, and infrared spectroscopy [27–31], i.e. at zero momentum transfer. All these methods demonstrated several gaps in the zone center ($q = 0$).

In the present paper, we report on spin dynamics of $NdFe_3(BO_3)_4$ explored by inelastic neutron scattering up to ~10 meV.

The crystal structure of this ferroborate is complicated (Fig. 1a) and corresponds to the space group R32. The iron atoms form chains around the screw-axis of the R32 space group, surrounded by tilted and slightly distorted oxygen octahedra. The octahedra are linked by edges via two oxygen atoms, giving rise to strongest super-exchange. The twisted chains are linked through planar BO_3 units giving rise to inter-chain interactions. The boron units are almost parallel to the *ab*-plane and intersect Fe layers along the *c*-axis. The central boron unit between the three chain sections, with equidistant oxygen atoms, links all neighbor Fe atoms from the three chains. This magnetic exchange is assisted by the additional pathways over slightly distorted BO_3 units in layers with +1/3 and −1/3 of the unit cell parameter along the *c*-axis.

The magnetic order of $NdFe_3(BO_3)_4$ was studied by neutron powder diffraction as well as single crystal diffraction [32,33]. An antiferromagnetic collinear structure of the "easy-plane" type, with the propagation vector $\mathbf{k} = [0\ 0\ 3/2]$ and magnetic moments within the basic plane appears at the Néel temperature of ~30 K. The magnetic order in the rare earth sublattice is induced by the magnetic order in the Fe sublattice.

Elastic neutron diffraction experiments demonstrate that the magnetic moments of Fe and Nd are aligned ferromagnetically in the basal plane, along with the *a*-axis [34]. These ferromagnetic layers alternate along the *c*-axis (Fig. 1b). Below ~13 K the collinear structure transforms to an incommensurate helical magnetic structure with the propagating vector along the *c*-axis.

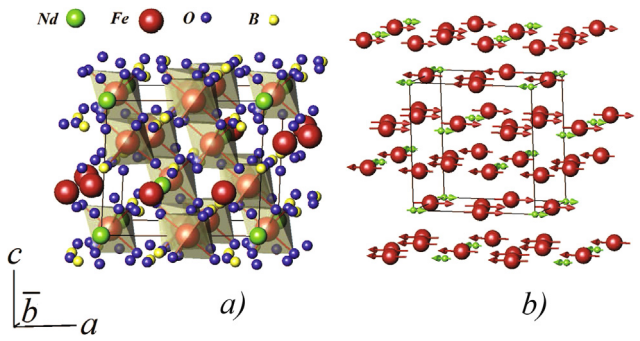

Fig. 1. (a) Atomic structure of $NdFe_3(BO_3)_4$. Atoms of Nd, Fe, O and B atoms are displayed in green, red, blue and yellow, respectively. (b) Magnetic structure at T = 13 K in the collinear phase. The unit cell is shown in a hexagonal setting. (For interpretation of the references to colour in this figure caption, the reader is referred to the web version of this article.)

2. Experiment

The inelastic scattering experiments were performed on the triple-axis spectrometers (TAS) ThALES and IN22 of Institut Laue-Langevin. A large single crystal of $NdFe_3(^{11}BO_3)_4$prepared at the Institute of Physics in Krasnoyarsk was used. This crystal was enriched with the isotope ^{11}B to decrease neutron absorption. It was mounted inside the so-called orange cryostat, providing sample temperatures in the range 1.5–300 K, and orientated with the reciprocal a^*- and c^*-axis in the scattering plane of the TAS.

The majority of scans were performed with a double focusing PG002 monochromator and a double focusing PG002 analyzer. We used a fixed final wavenumber of $k_f = 1.55$ Å^{-1} on TAS ThALES and $k_f = 2.662$ Å^{-1} on TAS IN22, leading to energy resolutions on the elastic line of $\delta E = 0.18$ meV and $\delta E = 0.8$ meV, respectively. Several scans close to the magnetic zone center were repeated with a Si111 monochromator and a lower final wavenumber of $k_f = 1.2$ Å^{-1} on TAS ThALES, with an improved energy resolution of $\delta E = 0.1$ meV. The replacement from PG002 to Si111 additionally improved the line shape of the elastic line, resulting in a perfect Gaussian shape.

A velocity selector upstream the monochromator position of TAS ThALES was used as a broadband neutron filter in order to suppress higher order contamination from the monochromator. For the same reason a PG002 filter was installed on TAS IN22 after the sample position.

Inelastic experiments were performed at temperature T = 15 K, in the commensurate phase, above the transition to the incommensurate phase, around the magnetic zone center (0 0 3/2), along the symmetry directions [0 0 ξ] and [ξ 0 1.5]. At this temperature, the thermal population of the bosonic magnons is small and the measurements were performed on the so-called "energy gain side" with the incident neutron energy larger than the final energy in order to create the magnetic excitations.

It should be noted that the incommensurate structure has very long period ~1000 Å, with the wave vector of the helix is $\mathbf{k} = [0\ 0\ 3/2 + \varepsilon]$, where $\varepsilon = 0.0074$ r.l.u. (reciprocal lattice unit) [34]. Such incommensurability is below the used instrumental *q*-resolution of the triple-axis spectrometer of $\delta q \sim 0.01$ Å^{-1}.

3. Experimental details and model calculations

The temperature dependences of the typical scans measured on TAS IN22 clearly show the distinct magnetic excitations observed up to 5 meV, which appear below the Néel temperature T_N ~30 K (Fig. 2). The shift of the magnon peaks to higher energies with decreasing temperature is due to the continuous increase of the magnetic moments, leading to a stiffening of the spin-wave branches close to the magnetic zone center.

In addition to the low-energy magnons (Fig. 2a), which were reported in Ref. [26], the high-energy excitations at about 4.5 MeV are clearly seen in the constant Q s can (Fig. 2b). They disappear above the Neel temperature that confirms their magnetic nature. The map of the dispersion spectra measured at TAS ThALES

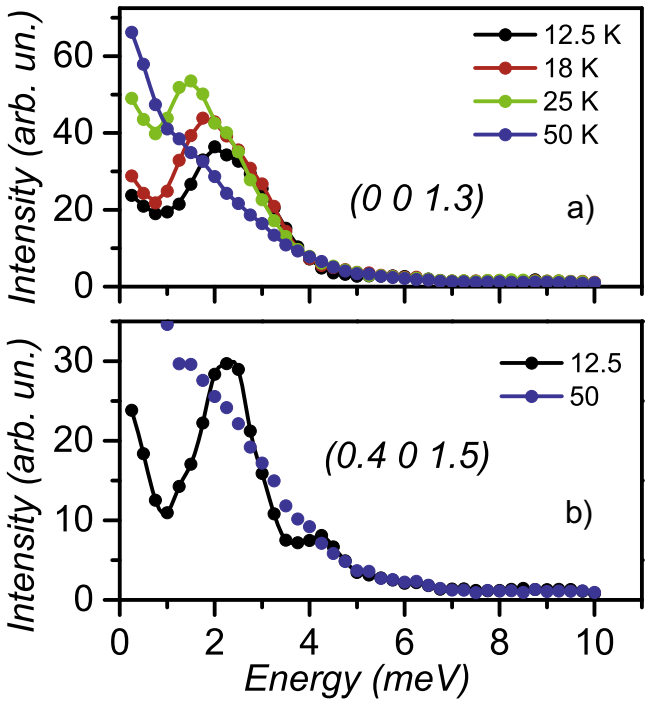

Fig. 2. Temperature dependence of the spectrum, measured at the points (0 0 1.3) (a) and (0.4 0 1.5) (b) in the reciprocal space.

along two principal directions [0 0 ξ] and [ξ 0 1.5] at temperature 15 K is shown in Fig. 3a and b, respectively.

In the crystal structure of $NdFe_3(BO_3)_4$ the Fe atoms occupy the 9d site with coordinates: (x, 0, 0); (0, x, 0) and (-x, -x, 0), (where x = 0.55), while the Nd atoms occupy the 3a site with coordinate (0, 0, 0). Keeping in mind the trigonal translations, there are 12 magnetic atoms in a chemical cell. Because the magnetic cell is twice the chemical cell, there are 24 non-equivalent magnetic moments, which should provide 24 dispersion branches.

The straightforward diagonalization of the interaction matrix of so large order is a time-consuming procedure and asks for a special approach. However, one can limit to four ferromagnetic sublattices: 3 sublattices of the Fe atoms and one sublattice of the Nd atoms. Turning to the bosonic creation and annihilation operators in a magnetic cell, we get the interaction matrix of 16 × 16, whose

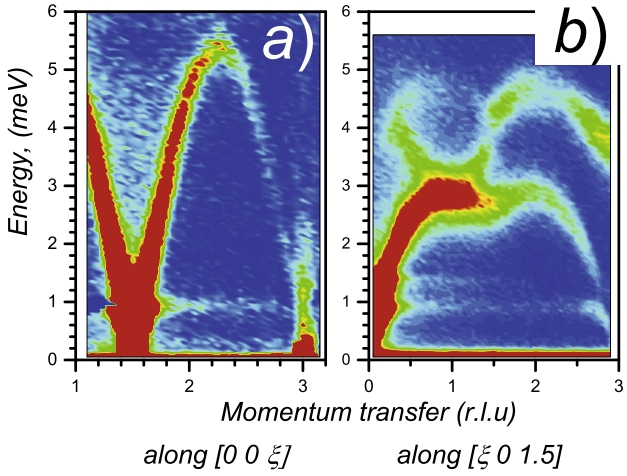

Fig. 3. Dispersion curves, measured on TAS ThALES at temperature 15 K along two principal directions [0 0 ξ] (a) and [ξ 0 1.5] (b), respectively.

eigenvalues are the energies of magnons. In isotropic approximation, this matrix represents two identical blocks of 8 × 8.

Diagonalization of the interaction matrix gives four twice-fold degenerate branches with a non-zero spectral weight. The analysis shows that the 24 branches can be constructed from these four branches, using the translations [1 0 0] and [2 0 0] (or [0 1 0] and [0 2 0] in the Q-space). This property could be easily understood by symmetry arguments, considering the trigonal translations, which connect the ferromagnetic planes, alternating along the *c*-axis.

However, instead of the straightforward diagonalization, we used numerical calculations by the SpinW package developed by Sándor Tóth [35], which calculate the dispersion curves and their spectral weights using the classical linear spin wave approach [36,37]. Some calculations were carried out by the similar package developed by Sylvain Petit [38].

In the simplest case of three strongest interactions, the Hamiltonian could be written as:

$$H = J_1 \sum_{Fe-Fe,nn} \vec{S}_i \vec{S}_j + J_2 \sum_{Fe-Fe,nnn} \vec{S}_i \vec{S}_j \quad (1)$$

$$+ \sum_{Fe-Nd,nn} \vec{S}_i \hat{J}_3 \vec{s}_j + D_{Fe} \sum_{Fe} \left(S_{ix}^2 + S_{iy}^2 \right) \quad (2)$$

Axis *x* is aligned along the crystallographic axis *a*, axis *z* is aligned along the hexagonal axis *c*. It is worth to note that in (1) each pair of coupled ions is counted once.

The exchange parameters J_1 and J_2 correspond to the strongest interactions in the Fe sublattice: the intra-chain interaction, the nearest neighbors, and inter-chain interaction, the next nearest neighbors. J_3 is an exchange integral between the nearest neighbors Fe^{3+} and Nd^{3+} moments (Fig. 4). In (1) the positive exchange parameters correspond to antiferromagnetic interactions, while negative exchange parameters correspond to ferromagnetic interactions.

The effective spin operators *S* and *s* correspond to the Fe^{3+} and the Nd^{3+} moments, which in the ground state are 5/2 and 1/2

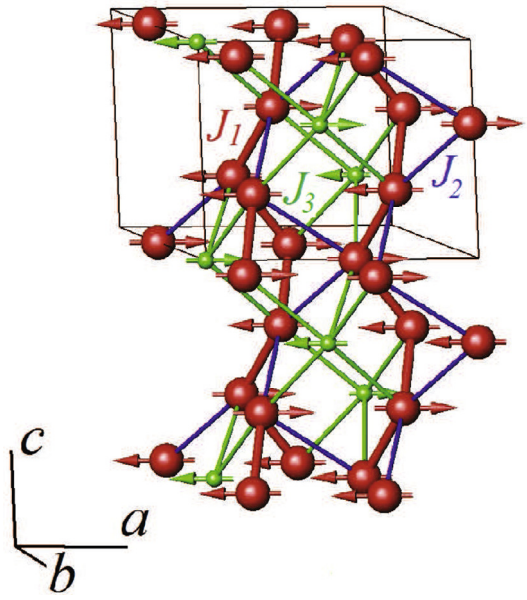

Fig. 4. Main magnetic pathways and corresponding interactions in $NdFe_3(BO_3)_4$. J_1 (in red) and J_2 (in blue) – antiferromagnetic exchange interactions between nearest and next nearest Fe ions, respectively. J_3 (in green) – antiferromagnetic exchange interaction between nearest Fe and Nd moments. (For interpretation of the references to colour in this figure caption, the reader is referred to the web version of this article.)

(Kramers doublet), respectively. However, because the spin dynamics measurements were performed at 15 K, in the calculation of the dispersion curves we used the static average spins, namely, $S_{Fe} = 2$ and $s_{Nd} = 0.25$, evaluated from the elastic neutron diffraction data at T = 15 K [33,34].

The averaged moment of Nd^{3+}, s_{Nd}, is induced by the exchange field of the Fe sublattice. Therefore, it depends on the Fe-Nd exchange parameter J_3 and, basically, it should be defined by the self-consistent procedure. The anisotropy of the Nd^{3+} g-factor and the anisotropy of the Fe-Nd exchange interaction could be simulated by the replacing of the exchange integral J_3 for the corresponding 3×3 matrix $\hat{J}_3$ with the non-zero diagonal terms only. The anisotropy of the Fe-Fe exchange parameters J_1 and J_2 could be represented by the matrices as well, however, these effects are beyond the accuracy of our experiment.

The parameter D_{Fe} defines an "easy-plane" anisotropy for Fe^{3+} ions. It could be presented in a form of a matrix with negative diagonal terms $D_{xx} = D_{yy}$ and $D_{zz} = 0$.

Additional exchange terms in the case of more interactions can be added in the formula (1) in an obvious way.

4. Results

The magnetic structure of $NdFe_3(BO_3)_4$ is governed by a large number of interactions, which are listed in Table 1 up to eight coordination sphere, with corresponding distances and the coordination numbers. At the first step, we restrict ourselves to the first four coordination spheres with the three strongest interactions J_1, J_2 and J_3. We neglect the interaction J_4, which connects the next nearest Fe and Nd neighbors in the basal plane. At this step, we do not account for anisotropy.

The fit by the SpinW package gives the next exchange parameters: $J_1 = 1.19$ meV, $J_2 = 0.14$ meV and $J_3 = 0.08$ meV, with an error of ~0.01 meV (Fig. 5). The analysis indicates that the low branch at about 1 meV in Fig. 5 (left panel, bottom) results from the Nd subsystem and is defined by the Fe-Nd interaction J_3. The clearly seen "branch repulsion" is obviously caused by the hybridization of the Nd and Fe excitations, i.e. electron transitions between the ground Nd $^{3+}$ Kramers doublet and acoustic Fe spin branch. Other branches are associated with the Fe spin dynamics.

It is seen that the strongest dispersion branches can be described in a satisfactory way, but the used set of the exchange parameters cannot describe the weak upper optical branches above ~3 meV along the [ξ 0 1.5] direction. It should be noted, the weak traces of these upper optical branches are seen in the map of the inelastic scattering reported in work [26] (Fig. 4), but they were remained out of attention.

Obviously, the model with three strongest interactions, which was accepted before [26,30] in is too simple and should be complemented by new interactions. Therefore, we expanded the range of the interactions, taking into consideration more coordination spheres.

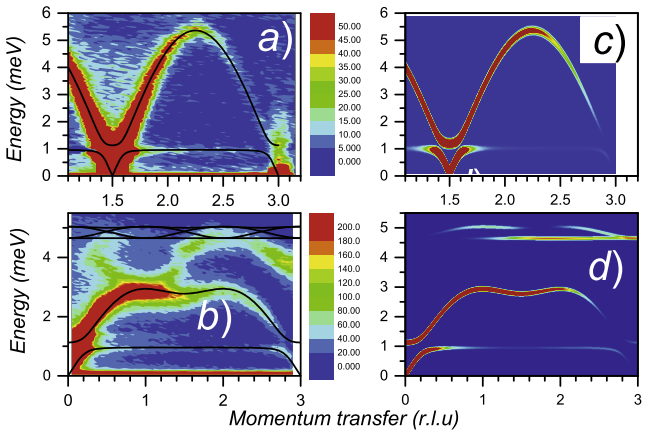

Fig. 5. Comparison of the measured dispersion curves with an experiment taking into account the three strongest interactions. Experimental maps of spin wave dispersion along [0 0 ξ] (a) and along [ξ 0 1.5] (c) measured at temperature 15 K. Black lines – the calculated dispersion curves. The branches with non-zero spectral weight are shown only. (b) and (d) – the calculated maps along [0 0 ξ] and [ξ 0 1.5] direction, respectively. (For interpretation of the references to colour in this figure caption, the reader is referred to the web version of this article.)

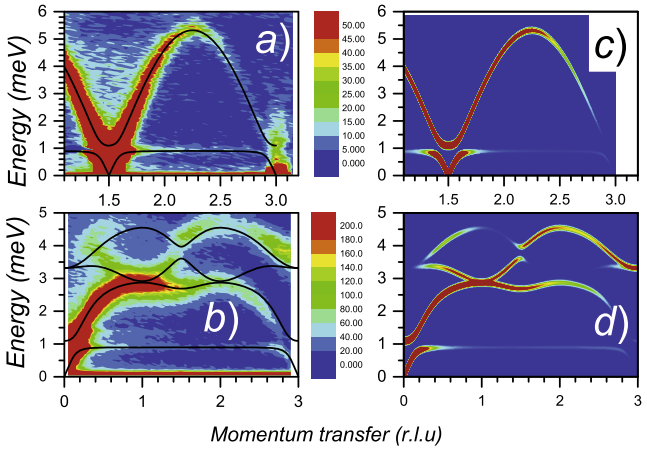

Fig. 6. Comparison of the measured dispersion curves with an experiment taking into account up to eight coordination spheres with (model 2 in Table 2). Experimental maps of spin wave dispersion along [0 0 ξ] (a) and along [ξ 0 1.5] (c) measured at temperature 15 K. Black lines – the calculated curves. The branches with non-zero spectral weight are shown only. Calculated maps along [0 0 ξ] (b) and along [ξ 0 1.5] (d). (For interpretation of the references to colour in this figure caption, the reader is referred to the web version of this article.)

It turned out that one can reasonably describe all observed branches, dispersion and the magnon intensities along two principal directions [0 0 ξ] and [ξ 0 1.5] (Fig. 6). The corresponding set of

Table 1
Interactions and coordination spheres (in order of increasing the radius of the sphere). In the calculations of distances the lattice parameters: a = 9.594 Å, c = 7.603 Å were used. z – coordination number.

NN	Label	Interaction	Distance (Å)	z
1	J_1	Fe-Fe, intra-chain	3.185	2
2	J_3	Fe-Nd, nearest neighbors	3.788	6
3	J_4	Fe-Nd, next nearest neighbors, in plane	4.312	3
4	J_2	Fe-Fe, inter-chain, nearest neighbors	4.409	2
5	J_5	Fe-Fe, inter-chain, next nearest neighbors, in plane	4.870	4
6	J_6	Fe-Fe along chains, next nearest neighbors	5.424	2
7	J_7	Fe-Nd, next nearest neighbors	5.796	3
8	J_8	Fe-Fe inter-chain, next nearest neighbors	6.091	6

Table 2
Exchange integrals for different models (meV).

Exchange integrals	Model 1*	Model 2*	Inelastic neutron scattering [26]**	Magnetic susceptibility and optical spectroscopy [30]
J_1 Fe-Fe	1.19	0.71	−0.482	0.54
J_3 Fe-Nd	0.08	0.04	0.008	0.04
J_4 Fe-Nd		−0.05		
J_2 Fe-Fe	0.14	0.17	−0.054	0.16
J_5 Fe-Fe		0.16		
J_6 Fe-Fe		−0.02		
J_8 Fe-Fe		0.14		

* An error of the exchange integral fit does not exceed 0.01 meV.
** It should note that in Ref. [26] the definition of the Hamiltonian is opposite by a sign to the definition, which is using in the presented work. Besides, instead of the effective magnetic moment s_{Nd}, the total angular moment J_{Nd} of Nd^{3+} was used in Ref. [26]. It results in the difference in the signs of the exchange parameters.

the exchange parameters is given in Table 2 (model 2) with the set of the three exchange parameters (model 1).

In the expanded model we took into consideration the next additional exchange parameters, which correspond to the interaction Fe-Fe in a basal plane J_5, the next nearest neighbors interaction Fe-Fe along the chains J_6 and the inter-chain interaction Fe-Fe J_8 (next nearest neighbors) (see Fig. 7). The induced Nd moment is eight times smaller than the Fe spin, therefore, the contribution of the Nd sublattice is very small. However, for generality, we considered the interaction Fe-Nd in a basal plane J_4, too. Here, we do not account for anisotropy.

From the analysis of the crystal structure it follows that the effective pathways corresponding to the interactions J_2, J_5 and J_8, through different BO_3 units, render similar exchanges. These additional interactions mainly account for the characteristic dispersion spectra along [ξ 0 1.5] direction in Fig. 6c. Other interactions, with distances above the eight coordination sphere radius, turned out to be an order of magnitude weaker and do not affect the spin-wave spectra.

In Table 2, the parameters reported in literature for $NdFe_3(BO_3)_4$ calculated in the frame of the model with three strongest interactions are presented for comparison. One set of parameters was obtained from the neutron inelastic scattering spectra in the collinear phase [26] (column 4). Another set of parameters was calculated from the magnetic susceptibility and the optical spectra [30] (column 5).

The distribution of the spectral weight along two principal directions contains detailed information, justifying the model 2. In Fig. 6 it is seen that the calculated positions of the high energy branches do not coincide properly with the experimentally observed ones. We attribute this discrepancy to the roughness of the linear spin-wave model.

The weak dispersionless branch, which is seen at about 1.4 meV on Fig. 3b could be associated with the transition between the exchange split levels of the Nd^{3+} Kramers doublet, which was observed by the absorption spectroscopy at 8.8 cm^{-1} (1.1 meV) [39] and in the Raman scattering [29].

In the crystal field, this doublet is well separated by an energy gap [30]. In the energy scans measured at the TAS IN22, there is a weak peak at high energies (Fig. 7), which does not show dispersion and is observed along all crystallographic directions. This excitation corresponds to the transition from the ground doublet to the first excited Nd^{3+} level, in agreement with optical measurements found this transition at 65 cm^{-1} (8.06 meV) [30].

5. Discussion

All exchange parameters, apart from weak J_4 and J_6, appeared to be positive, i.e. they render antiferromagnetic interactions. I.e. the magnetic ground state, stabilized by these interactions, is robust and stable against by the inclusion of small ferromagnetic interactions J_4 and J_6.

Remarkably, that the interaction J_5, which connects the parallel moments in the basal plane appears to be antiferromagnetic. The reason for the parallel orientation of the moments within the ferromagnetic planes lies in the peculiarity of the discussed structure (see Fig. 8). The total sum of the intra-chain interaction J_1 and the inter-chain interactions J_2 and J_8, which couple the magnetic moments from the adjacent ferromagnetic planes, overcomes the antiferromagnetic interaction J_5 between the moments within a plane, thus forcing the moments i n a layer to be parallel. This situation is rather unusual and stems from the complex structure of the magnetic surrounding.

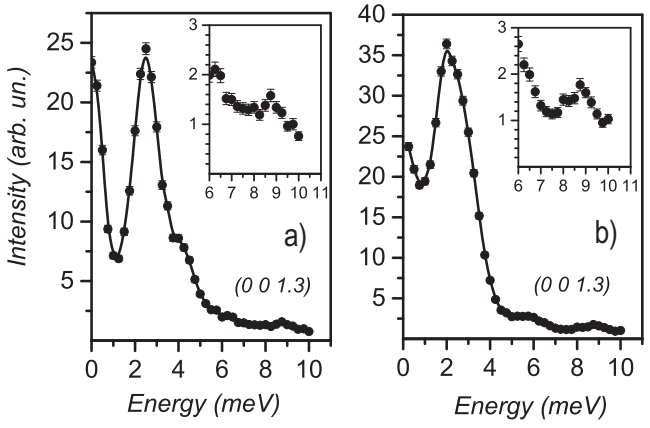

Fig. 7. Typical spectra measured at the points of reciprocal space 0.5 0 1.5 (a) and 0 0 1.3 (b) at 12.5 K at TAS IN22. In inserts, the enlarged fragments of the spectra are shown.

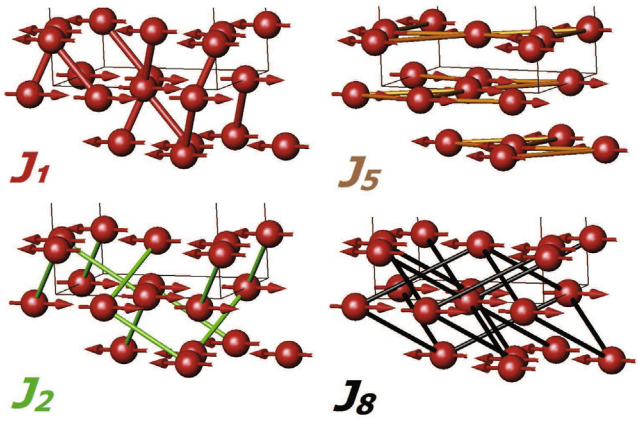

Fig. 8. Magnetic pathways corresponding to the interactions J_1, J_2, J_5, and J_8 in the Fe sublattice.

In Table 2 it is seen that all exchange integrals, which correspond to antiferromagnetic interactions are large: about of 20% of the strongest exchange integral. At the same time, the ferromagnetic interactions J_4 and J_6) are weaker: ~3–5% from the strongest interaction. This is consistent with the general concept of the interactions by the orbital overlapping, known as Kanamori-Goodenough rules: superexchange interactions depend on the orbital overlapping [40]. Indeed, from the crystal structure analysis, it follows that the exchange pathways via B and O atoms, which corresponds to the ferromagnetic connections, are distant and complicated. By contrast, the antiferromagnetic interactions are direct over BO_3 units. Note, the distance from the Fe ion to the nearest neighbors in the adjacent layers (interaction J_2) is shorter than the distance between Fe moments in a plane (interaction J_5), but the interactions J_2 and J_5 are similar by the strength.

Summarizing, the refinement of the spin-wave spectra demonstrates that there are four strong antiferromagnetic interactions in the Fe sublattice, which define the magnetic state: one strongest intra-chain interaction and three nearly inter-chain interactions.

In order to describe the low-energy part of the spin-wave spectra, one needs to account for the anisotropy of the magnetic interactions. The anisotropy originates from two reasons: an "easy-plane" anisotropy of Fe moments and an anisotropy related to the splitting of the Nd^{3+} Kramers doublet by the Nd-Fe exchange effective field. The latter is realized in the spin-wave spectra through Fe-Nd interactions.

The quasi-optical Thz-spectroscopy measurements at $q = 0$ have revealed several resonance modes in $NdFe_3(BO_3)_4$, namely, at 1.21 meV and at 1.25 meV, which were associated with Nd-excitations, and the resonances of 0.42 meV and at ~ zero energy, associated with excitations in Fe sublattice [27]. Antiferromagnetic resonance also showed the similar values for the gaps, associated with Fe sublattice: 0.421 meV and 0.0098 meV [31].

Using effective molecular field approach, we can estimate the exchange parameter J_3 via the relation:

$$J_3^{xx(zz)} = \Delta_{xx(zz)}/2 \cdot z \cdot S_{Fe}(T) \quad (3)$$

Here, Δ_{xx} and Δ_{zz} are the exchange splitting of the ground Nd^{3+} doublet for Fe moment $S_{Fe}(T)$ aligned within the *ab*-plane or along the *c*-axis, respectively; z = 6 is the coordination number. Using the splitting, measured by THz-spectroscopy [27] the following parameters of anisotropic Nd-Fe interactions are estimated: $J_3^{xx} = J_3^{yy} =$ 0.045 meV and $J_3^{zz} = 0.0475$ meV. The instrumental resolution was not enough to resolve the corresponding branches, but these values are close to the average refined parameter $J_3 = 0.04(1)$ meV in isotropic approximation.

The static average value of the effective spin $s(T)$ of Nd^{3+} is determined by Nd-Fe exchange and strongly depends on temperature. In the molecular field approximation, in the "easy-plane" state it can be expressed as follows [27]:

$$s(T) = 0.5 \cdot tanh(J_3 \cdot z \cdot S_{Fe}(T)/k_B T) \quad (4)$$

Here, $S_{Fe}(T)$ is the average Fe spin, which value is ≈2 at T = 15 K, k_B – the Boltzmann constant. Using the refined exchange parameter $J_3 = 0.04$ meV, $s(T) = 0.22$. The latter is very close to the parameter $s = 0.25$ used in the spin-wave calculation, that confirms the reliability of the refined exchange parameter of J_3.

To get further insight into the anisotropy, the measurements around the zone center (0 0 1.5) with the improved energetic resolution were performed (Fig. 9). Our instrumental resolution was not enough to resolve the dispersion branches near the zone center because of the strong elastic line. We observe two unresolved peaks, which averaged positions are shown by white points in Fig. 9.

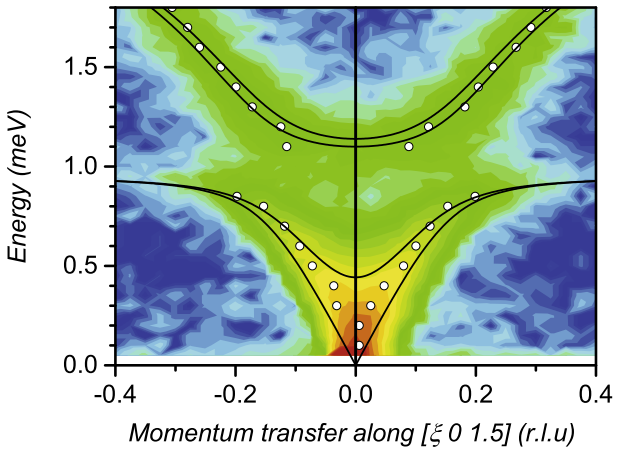

Fig. 9. The low energy spin-wave spectrum around the zone center (0 0 1.5) with an improved energy resolution, measured at TAS ThALES. White spots correspond to the positions of the lowest energetic branches, fitted from the decomposition of the energy scans for Gaussians. Calculated dispersion curves, taking into account "in-plane" anisotropy with $D = -0.007$ meV, are shown in black lines. (For interpretation of the references to colour in this figure caption, the reader is referred to the web version of this article.)

The anisotropy of the exchange parameter of J_3 is beyond our resolution. The "in-plane" anisotropy is described by the diagonal terms $D_{xx} = D_{yy} = D$ and $D_{zz} = 0$. For calculation of the dispersion curves we used $D = -0.007$ meV, which corresponds to a reported AFM and Thz-spectroscopy resonance of 0.42 meV, associated with the Fe sublattice [27,31]. In Fig. 9 it is seen that $D = -0.007$ meV is too small in contrast with the exchange parameters to be fitted reliably.

6. Conclusion

Inelastic neutron scattering experiments were performed in ferroborate $NdFe_3(BO_3)_4$ to assess the magnetic excitations and to obtain the exchange parameters in the collinear antiferromagnetic phase. The observed spectra were analyzed in the frame of the linear spin-wave theory based on the magnetic structure, derived from the elastic neutron scattering.

It was shown that to describe adequately all observed dispersion curves three basic interactions: between the nearest and the next nearest neighbors in Fe sublattice and an interaction Fe-Nd is not enough. It is necessary to take into consideration up to eight coordination spheres. Remarkably, only four antiferromagnetic interactions: the intra-chain interaction (the nearest neighbors) and three near inter-chain interactions play a role. Other interactions appeared to be insignificant.

Taking into account the expanded number of interactions, one can draw an important conclusion. The refinement shows that the exchange between the Fe spins in the ferromagnetic plane (5-th coordination sphere) appeared to be antiferromagnetic and therefore it cannot provide a parallel arrangement alone. Such arrangement is supported by the antiferromagnetic exchanges between the Fe spins in the adjacent ferromagnetic layers (4-th and 8-th coordination spheres).

It demonstrates that the pathway geometry in a complex crystal structure plays more important role in the stabilization of the magnetic structure than an inter-atomic distance.

Acknowledgement

We are grateful to J. Kulda, A. Ivanov, V. Skumryev and S. Petit for fruitful discussions. The work was supported by the Russian

grants RFBR 16-02-00058, RFBR 15-02-07647 and RG 14. B25.31.0025.

References

[1] G.A. Smolenskii, I.E. Chupis, Sov. Phys. Uspekhi 25 (1982) 475.
[2] T. Kimura, G. Lawes, T. Goto, Y. Tokura, A.P. Ramirez, Phys. Rev. B 71 (2005) 224425.
[3] M. Kenzelmann, A.B. Harris, S. Jonas, C. Broholm, J. Schefer, S.B. Kim, C.L. Zhang, S.-W. Cheong, O.P. Vajk, J.W. Lynn, Phys. Rev. Lett. 95 (2005) 087206.
[4] T. Goto, T. Kimura, G. Lawes, A.P. Ramirez, Y. Tokura, Phys. Rev. Lett. 92 (2004) 257201.
[5] A. Inomata, K. Kohn, J. Phys.: Condens. Matter 8 (1996) 2673.
[6] J. Hemberger, F. Schrettle, A. Pimenov, P. Lunkenheimer, V.Yu. Ivanov, A.A. Mukhin, A.M. Balbashov, A. Loidl, Phys. Rev. B 75 (2007) 035118.
[7] N. Hur, S. Park, P.A. Sharma, J.S. Ahn, S. Guha, S.-W. Cheong, Nature 429 (2004) 392.
[8] G. Lawes, A.B. Harris, T. Kimura, N. Rogado, R.J. Cava, A. Aharony, O. Entin-Wohlman, T. Yildirim, M. Kenzelmann, C. Broholm, A.P. Ramirez, Phys. Rev. Lett. 95 (2005) 087205.
[9] R. Ramesh, N.A. Spaldin, Nat. Mater. 6 (2007) 21.
[10] A.K. Zvezdin, S.S. Krotov, A.M. Kadomtseva, G.P. Vorob'ev, Yu.F. Popov, A.P. Pyatakov, L.N. Bezmaternykh, E.A. Popova, JETP Lett. 81 (2005) 272.
[11] F. Yen, B. Lorenz, Y.Y. Sun, C.W. Chu, L.N. Bezmaternykh, A.N. Vasiliev, Phys. Rev. B 73 (2006) 054435.
[12] A.K. Zvezdin, G.P. Vorob'ev, A.M. Kadomtseva, Yu.F. Popov, P. Pyatakov, L.N. Bezmaternykh, A.V. Kuvardin, E.A. Popova, JETP Lett. 83 (2006) 509.
[13] A.A. Mukhin, G.P. Vorob'ev, V.Yu. Ivanov, A.M. Kadomtseva, A.S. Narizhnaya, A. M. Kuz'menko, Yu.F. Popov, L.N. Bezmaternykh, A. Gudim, JETP Lett. 93 (2011) 275.
[14] K.-C. Liang, R.P. Chaudhury, B. Lorenz, Y.Y. Sun, L.N. Bezmaternykh, V.L. Temerov, C.W. Chu, Phys. Rev. B 83 (2011) 180417.
[15] A.M. Kadomtseva, Yu.F. Popov, G.P. Vorob'ev, A.P. Pyatakov, S.S. Krotov, K.I. Kamilov, V.Yu. Ivanov, A.A. Mukhin, A.K. Zvezdin, A.M. Kuz'menko, L.N. Bezmaternykh, I.A. Gudim, V.L. Temerov, Low Temp. Phys. 36 (2010) 511.
[16] A. Pimenov, A.A. Mukhin, V.Yu. Ivanov, V.D. Travkin, A.M. Balbashov, A. Loidl, Nat. Phys. 2 (2006) 97.
[17] A.M. Kuzmenko, A. Shuvaev, V. Dziom, Anna Pimenov, M. Schiebl, A.A. Mukhin, V.Yu. Ivanov, L.N. Bezmaternykh, A. Pimenov, Phys. Rev. B 89 (2014) 174407.
[18] A.A. Mukhin, A.M. Kuzmenko, V. Yu Ivanov, A.G. Pimenov, A.M. Shuvaev, V.E. Dziom, Russ. Phys. – Uspekhi 58 (10) (2015) 993.
[19] A.M. Kuzmenko, V. Dziom, A. Shuvaev, Anna Pimenov, M. Schiebl, A.A. Mukhin, V.Yu. Ivanov, I.A. Gudim, L.N. Bezmaternykh, A. Pimenov, Phys. Rev. B 92 (2015) 184409.
[20] J. Jeong, E.A. Goremychkin, T. Guidi, K. Nakajima, Gun Sang Jeon, Shin-Ae Kim, S. Furukawa, Yong Baek Kim, Seongsu Lee, V. Kiryukhin, S-W. Cheong, Je-Geun Park, Phys. Rev. Lett. 108 (2012) 077202.
[21] H. Ehrenberg, H. Weitzel, H. Fuess, B. Hennion, J. Phys.: Condens. Matter 11 (1999) 2649.
[22] Feng Ye, R.S. Fishman, J.A. Fernandez-Baca, A.A. Podlesnyak, G. Ehlers, H.A. Mook, Yaqi Wang, B. Lorenz, C.W. Chu, Phys. Rev. B 83 (2011) 140401(R).
[23] X. Fabréges, S. Petit, I. Mirebeau, S. Pailhés, L. Pinsard, A. Forget, M.T. Fernandez-Diaz, F. Porcher, Phys. Rev. Lett. 103 (2009) 067204.
[24] T. Chatterji, Pramana 71 (4) (2008) 847.
[25] D. Senff, P. Link, K. Hradil, A. Hiess, L.P. Regnault, Y. Sidis, N. Aliouane, D.N. Argyriou, M. Braden, Phys. Rev. Lett. 98 (2007) 137206.
[26] S. Hayashida, M. Soda, S. Itoh, T. Yokoo, K. Ohgushi, D. Kawana, H.M. Rnnow, T. Masuda, Phys. Rev. B 92 (2015) 054402.
[27] A.M. Kuzmenko, A.A. Mukhin, V.Yu. Ivanov, A.M. Kadomtseva, L.N. Bezmaternykh, JETP Lett. 94 (2011) 294.
[28] A.M. Kuzmenko, A.A. Mukhin, V.Y. Ivanov, L.N. Bezmaternikh, Solid State Phenom. 190 (2012) 269.
[29] D. Fausti, A.A. Nugroho, P.H.M. van Loosdrecht, S.A. Klimin, M.N. Popova, L.N. Bezmaternykh, Phys. Rev. B 74 (2006) 024403.
[30] M.N. Popova, E.P. Chukalina, T.N. Stanislavchuk, B.Z. Malkin, A.R. Zakirov, E. Antic-Fidancev, E.A. Popova, L.N. Bezmaternykh, V.L. Temerov, Phys. Rev. B 75 (2007) 224435.
[31] M.I. Kobets, K.G. Dergachev, E.N. Khatsko, S.L. Gnatchenko, L.N. Bezmaternykh, V.L. Temerov, Physica B 406 (2011) 3430.
[32] P. Fischer, V. Pomjakushin, D. Sheptyakov, L. Keller, M. Janoschek, B. Roessli, J. Schefer, G. Petrakovskii, L. Bezmaternikh, V. Temerov, D. Velikonov, J. Phys.: Condens. Matter 18 (2006) 7975.
[33] M. Janoschek, P. Fischer, J. Schefer, B. Roessli, V. Pomjakushin, M. Meven, V. Petricek, G. Petrakovskii, L. Bezmaternikh, Phys. Rev. B 81 (2010) 094429.
[34] I.V. Golosovsky, E. Ressouche, unpublished, 2016.
[35] Sándor Tóth, www.psi.ch/spinw; S. Tóth, B. Lake, arXiv: 1402.6069.
[36] F. Bloch, Zeitschrift fur Phys. 61 (1930) 206.
[37] J.C. Slater, Phys. Rev. 35 (1930) 509.
[38] S. Petit, Collection Société Française de Neutrons 12 (2011) 105.
[39] E.P. Chukalina, D.Yu. Kuritsin, M.N. Popova, L.N. Bezmaternykh, S.A. Kharlamova, V.L. Temerov, Phys. Lett. A 322 (2004) 239.
[40] J. Goodenough, Magnetism and the Chemical Bond, Inter-science Publishers, NY, 1963.